Large Topological Hall Effect in a Short-Period Helimagnet MnGe

N. Kanazawa,[1] Y. Onose,[1,2] T. Arima,[3,4] D. Okuyama,[5] K. Ohoyama,[6] S. Wakimoto,[7] K. Kakurai,[7] S. Ishiwata,[1] and Y. Tokura[1,2,5]

[1]*Department of Applied Physics and Quantum Phase Electronics Center (QPEC), University of Tokyo, Tokyo 113-8656, Japan*
[2]*Multiferroics Project, ERATO, Japan Science and Technology Agency (JST), Tokyo 113-8656, Japan*
[3]*Institute of Multidisciplinary Research for Advanced Materials, Tohoku University, Sendai 980-8577, Japan*
[4]*RIKEN SPring-8 Center, Sayo, Hyogo 679-5148, Japan*
[5]*Cross-Correlated Materials Research Group (CMRG) and Correlated Electron Research Group (CERG), RIKEN Advanced Science Institute, Wako 351-0198, Japan*
[6]*Institute for Materials Research, Tohoku University, Sendai 980-8577, Japan*
[7]*Quantum Beam Science Directorate, Japan Atomic Energy Agency, Tokai, Ibaraki 319-1195, Japan*

(Received 26 January 2011; published 15 April 2011)

We have observed an unconventional, likely topological, Hall effect over a wide temperature region in the magnetization process of a chiral-lattice helimagnet MnGe. The magnitude of the topological Hall resistivity is nearly temperature-independent below 70 K, which reflects the real-space fictitious magnetic field proportional to a geometric quantity (scalar spin chirality) of the underlying spin texture. From the neutron diffraction study, it is anticipated that a relatively short-period (3–6 nm) noncoplanar spin structure is stabilized from the proper screw state in a magnetic field to produce the largest topological Hall response among the B20-type (FeSi-type) chiral magnets.

DOI: 10.1103/PhysRevLett.106.156603 PACS numbers: 72.15.Gd, 72.25.Ba, 75.25.−j, 75.30.−m

Finding a novel electromagnetic phenomenon out of a topological spin texture has become an attracting subject in condensed matter physics. Especially, the spin chirality is one of the key notions to produce new phenomena in a spin-charge coupled system. For example, it has been well established [1] that the magnetic states with a finite vector spin chirality $\boldsymbol{S}_i \times \boldsymbol{S}_j$ such as transverse helical magnets host the electric polarization. The magnetically induced ferroelectricity has been attracting much attention because of its gigantic magnetoelectric response. On the other hand, itinerant magnets with a scalar spin chirality $\boldsymbol{S}_i \cdot (\boldsymbol{S}_j \times \boldsymbol{S}_k)$ provide another interesting laboratory. While hopping over three sites with localized spin moments ($\boldsymbol{S}_i$, $\boldsymbol{S}_j$, and $\boldsymbol{S}_k$), the conduction electron collects a phase factor, i.e., Berry phase, proportional to the scalar spin chirality. The fictitious magnetic field caused by the Berry phase may induce a nontrivial Hall effect as termed topological Hall effect (THE) [2–5].

The effect of Berry phase due to spin chirality is frequently canceled out by the sum over the whole lattice sites in real materials. Onoda *et al.* [4] pointed out that there are two mechanisms to avoid such cancellation and to induce THE. One is caused by the presence of inequivalent multiple loops in a unit cell. In this case, even if the total spin chirality is zero, the electrons acquire the Berry phase in the course of momentum change. The topological Hall effect induced by this mechanism has been observed for pyrochlores $Nd_2Mo_2O_7$ [6] and $Pr_2Ir_2O_7$ [7]. The other mechanism is due to the spin texture hosting the spin chirality, whose size is much larger than the lattice constant. One such example is a topological spin texture called Skyrmion, in which the varying direction of the spins wraps a sphere. In the continuum limit, the total spin chirality is proportional to the number of the Skyrmion. The momentum-space fictitious magnetic field $\boldsymbol{b}_k$ in the former case gives rise to the so-called anomalous velocity $\boldsymbol{v} = \frac{e}{\hbar}\boldsymbol{E} \times \boldsymbol{b}_k$. In this case, Hall *conductivity* is expressed as $\sigma_{xy} = \frac{e^2}{\hbar}\Sigma f(\epsilon) b_{kz}$ ($f(\epsilon)$ is Fermi distribution function), being independent of the scattering rate $1/\tau$. In ferromagnets, the spin-orbit interaction also gives rise to $\boldsymbol{b}_k$ and induces the anomalous Hall effect (AHE) proportional to the magnetization [2,8]. By contrast, the real-space fictitious magnetic field $\boldsymbol{b}_r$ in the latter case is expected to give rise to the fictitious Lorentz force $F = e\boldsymbol{v} \times \boldsymbol{b}_r$ and Hall *resistivity* $\rho_{yx} = R_0 b_{rz}$, where the normal Hall coefficient R_0 is independent of $1/\tau$. This relation has, however, scarcely been examined experimentally so far.

It was anticipated that the crystallization of the Skyrmion spin textures can be realized in helimagnets with B20 crystal structure [9–11]. Recently, small angle neutron scattering studies have detected the formation of a triangular lattice of Skyrmions in a narrow temperature magnetic field (T-H) window just below T_N in B20-type MnSi, $Fe_{1-x}Co_xSi$, and $Mn_{1-x}Fe_xSi$ [12–14]. Furthermore, the real-space observation for $Fe_{0.5}Co_{0.5}Si$ and FeGe by Lorentz transmission electron microscopy [15,16] has clearly demonstrated the spin configuration of Skyrmion cyrstal (SkX). A topological Hall effect, assigned to the outcome of SkX, has already been observed in MnSi at ambient pressure [17] and high pressure [18]. However, the Hall anomaly remains very small and appears in a very narrow temperature region ($|\rho_{yx}^T| \approx 4$ nΩ cm and

$T = 28$–29 K at ambient pressure); therefore the nature of the THE, such as the $1/\tau$ dependence, remains veiled. In this paper, we report the observation of a large THE in B20-type MnGe possibly with the maximal density of Skyrmion. The Hall anomaly assigned to the THE is observed in a much wider T-H region than in MnSi. Almost T-independent topological Hall resistivity seems to be caused by the real-space fictitious magnetic field due to the short-period ($\approx$ 3–6 nm) crystallization of spin texture with scalar spin chirality.

MSi and MGe (M: transition metal) crystalize into a cubic B20-type structure with noncentrosymmetric space group $P2_13$. Some of them, such as MnSi, $Fe_{1-x}Co_xSi$, and FeGe, show a long-period ($\lambda = 18$–90 nm) helical spin structure [19–21] due to the competition between ferromagnetic exchange interaction J and Dzyaloshinsky-Moriya interaction D, where the ratio J/D determines the helical period λ [22,23]. As the magnetic anisotropy is very weak, all the helical orders in different directions are almost energetically degenerate. The Skyrmion crystal state with the nearly identical lattice constant to λ is stabilized at finite magnetic fields just below T_N by the interference of threefold helices with their modulation vectors perpendicular to the applied field [12]. B20-type MnGe, as investigated in this study, can be synthesized only under a high pressure. MnGe shows an antiferromagnetic M-T curve with $T_N \approx 170$ K, but its helimagnetic structure was not proved [24].

The polycrystalline samples of B20-type MnGe were synthesized with a cubic-anvil-type high-pressure apparatus. A mixture of elemental materials with an atomic ratio of 1:1 was at first arc-melted in an argon atmosphere. The alloy was placed in a cylindrical BN capsule and was heat-treated for 1 h at 1073 K under a high pressure of 4 GPa. Samples for transport and magnetization measurements were cut into rectangular shape with a typical size of $4 \times 1.5 \times 0.2$ mm^3. Measurements of magnetoresistance and Hall resistivity were performed with the current parallel to the longest side (x axis) and the magnetic field to the shortest one (z axis). Magnetization (M) was measured with the same magnetic-field direction as the transport measurements. Powder neutron diffraction experiments were performed using HERMES and TAS-2 installed at the JRR-3 reactor of the Japan Atomic Energy Agency (JAEA). The powder sample includes a trace of impurity less than 4% in volume fraction.

Figure 1(a) shows the T dependence of resistivity and susceptibility of MnGe. The resistivity exhibits metallic a behavior with the residual resistance ratio $\rho(300\text{ K})/\rho(2\text{ K}) \approx 19$, while the susceptibility shows a broad antiferromagnetic peak around $T_N \approx 170$ K. Shown in the inset of Fig. 1(b) are the neutron diffraction patterns around (110) reflection at various temperatures as subtracted by the profile at 270 K. Two new peaks of magnetic origin were discerned at each temperature below T_N.

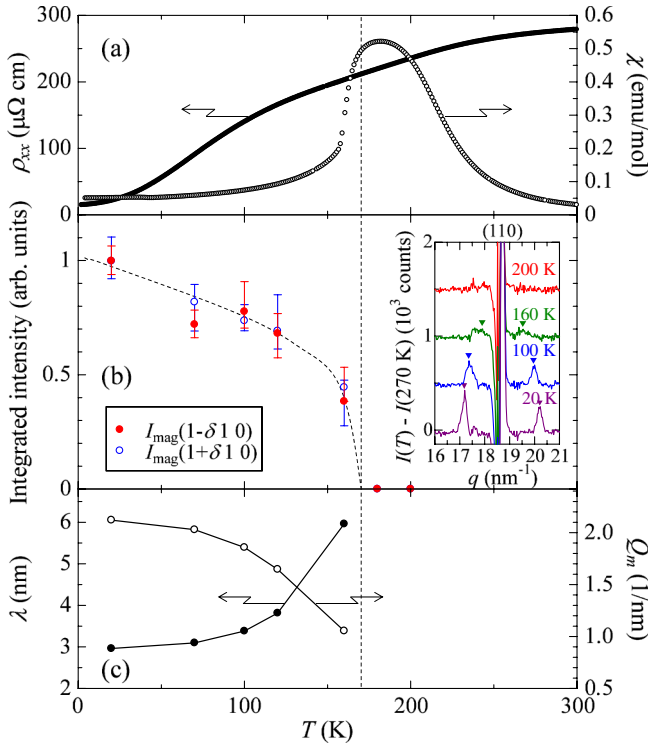

FIG. 1 (color online). (a) Temperature dependence of resistivity and magnetic susceptibility ($\chi = M/H$ at $H = 100$ Oe) in MnGe. (b) Temperature dependence of the integrated intensity of magnetic Bragg peaks indexed with the propagation vector $\boldsymbol{Q}_m = \{\delta 00\}$. The integrated intensity is normalized by that at 20 K. Inset shows neutron powder diffraction patterns of 20, 100, 160, and 200 K as subtracted by that at 270 K $> T_N$. (c) Temperature dependence of the helical period λ and the magnitude of $\boldsymbol{Q}_m$. The dashed and solid lines in (b) and (c) are the guide to the eyes.

The integrated intensity of these reflections decreases with increasing temperature and finally disappears above T_N [Fig. 1(b)]. Two and four magnetic peaks also appear around (111) and (210) reflections, respectively. Since a magnetic reflection, in general, appears at $|\boldsymbol{q}| = |\boldsymbol{Q} \pm \boldsymbol{Q}_m|$ in a powder neutron diffraction pattern, these magnetic peak positions can be accounted for with an incommensurate helical magnetic structure with $\boldsymbol{Q}_m = \{\delta 00\}$; the magnetic peaks around (110), (111), and (210) reflections are indexed as $\boldsymbol{q} = \{1 \pm \delta 10\}$, $\boldsymbol{q} = \{1 \pm \delta 11\}$, and $\boldsymbol{q} = \{2 \pm \delta 10\}$, $\{1 \pm \delta 20\}$, respectively. Here we define $\boldsymbol{q}$, $\boldsymbol{Q}$, and $\boldsymbol{Q}_m$ as the scattering vector, the reciprocal lattice vector, and the magnetic modulation vector, respectively. The helical period varies from 6 to 3 nm with decrease of temperature, which is the shortest among the known B20-type helimagnets [Fig. 1(c)], promising the highest-density Skyrmions if realized in a magnetic field.

Figure 2 shows the magnetic-field dependence of M, magnetoresistance $\rho_{xx}(H)/\rho_{xx}(0)$, and Hall resistivity ρ_{yx}. The magnetization curve shows a kink representing the transition to the induced ferromagnetic state. We define

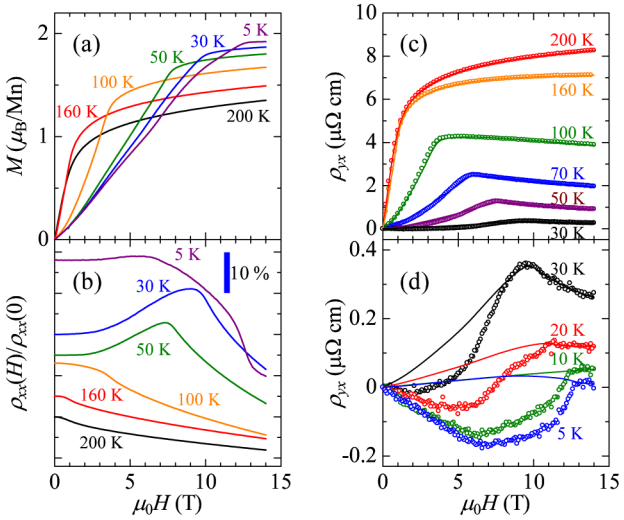

FIG. 2 (color online). Magnetic-field dependence of (a) magnetization M, (b) resistivity ρ_{xx} as normalized by the zero-field value $\rho_{xx}(0)$, and (c),(d) Hall resistivity ρ_{yx} at various temperatures. Solid lines in panels (c) and (d) are the fitted curves of ρ_{yx} using the relation that $\rho_{yx} = R_0 B + S_A \rho_{xx}^2 M$ with the fitting parameters R_0 and S_A (see text).

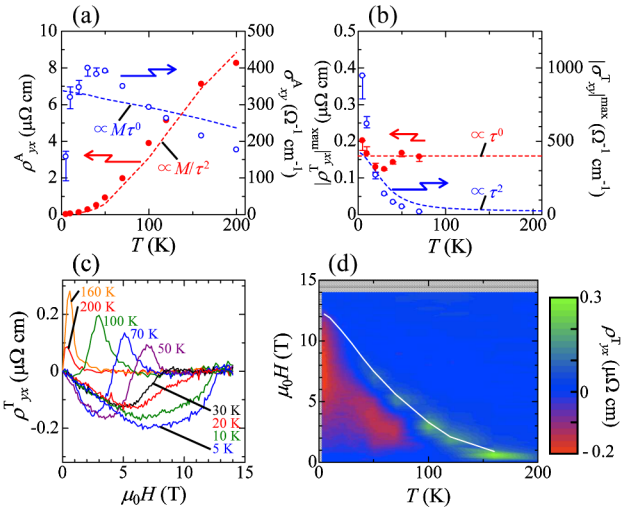

FIG. 3 (color online). (a) and (b) Comparison between T-dependence of (a) anomalous and (b) topological components of Hall resistivity (solid circles) and conductivity (open circles). ρ^A_{yx} is here defined by the value of ρ_{yx}(14 T), while $|\rho^T_{yx}|^{max}$ here by the negative maximal values of ρ^T_{yx}-H curves in panel (c). (c) Magnetic-field dependence of topological Hall resistivity ρ^T_{yx}. (d) A contour map of ρ^T_{yx} in the plane of temperature and magnetic field. The white curve represents the temperature variation of the critical field H_C, at which the ferromagnetic spin-collinear state is realized.

the kink field as the critical field H_C. A Hall anomaly, which deviates from the shape of the magnetization curve, becomes increasingly conspicuous below 30 K, where the sign change of ρ_{yx} is observed. An additional component of the Hall effect produces a negative value of ρ_{yx} besides AHE and B-linear normal Hall effect (NHE), which we attribute to THE. To estimate this additional part ρ^T_{yx}, we assume the relation,

$$\rho_{yx} = \rho^N_{yx} + \rho^A_{yx} + \rho^T_{yx} = R_0 B + S_A \rho^2_{xx} M + \rho^T_{yx}. \quad (1)$$

Here, the term $S_A \rho^2_{xx}$ ($\mu_0 R_S$) corresponds to the AHE coefficient; the anomalous Hall *conductivity* (σ^A_{xy}) is M-linear and hence we anticipate that S_A is an H-independent parameter [25]. As the topological Hall resistivity should vanish when the ferromagnetic spin-collinear state is induced at $H > H_C$, we can determine R_0 and S_A as the slope and the intercept of the curve ρ_{yx}/B vs $\rho^2_{xx} M$ above the critical field H_C. As shown in Figs. 2(c) and 2(d), we obtained a good fit above H_C with the fitting parameters R_0 and S_A; above H_C, the magnetoresistance [a decrease of ρ_{xx}, Fig. 2(b)] is important to explain a decrease of Hall resistivity through the anomalous Hall term $S_A \rho^2_{xx}$. As a result of the fitting, the additional contribution ρ^T_{yx} is estimated as the subtraction of $\rho^N_{yx} + \rho^A_{yx}$ from measured ρ_{yx} [Fig. 3(c)]. Note that a peak shape of ρ^T_{yx} around H_C above 50 K is perhaps not essential but merely a byproduct; this is due to difficulty in estimate of the small ρ^T_{yx} buried in the much larger ρ^A_{yx}, which increases in proportion to ρ^2_{xx} with increasing temperature. Nevertheless, we can obtain valid estimation below 70 K as is evident also from the raw data shown in Fig. 2(d).

We find almost constant quantity, $\rho^T_{yx} \approx -0.16\ \mu\Omega$ cm, against temperature variation below 70 K. This temperature independence is the key for the topological feature of ρ^T_{yx}. We show the T dependence of ρ^A_{yx} (σ^A_{xy}) and ρ^T_{yx} (σ^T_{xy}) in Figs. 3(a) and 3(b), where we plot ρ_{yx}(14 T) (σ_{xy}(14 T)) as ρ^A_{yx} (σ^A_{xy}) and the negative peak value of ρ^T_{yx} (σ^T_{xy}) as $|\rho^T_{yx}|^{max}$ ($|\sigma^T_{xy}|^{max}$), respectively. Both ρ^A_{yx} and ρ^T_{yx} are in good agreement with the anticipated relations, $\rho^A_{yx} = S_A \rho^2_{xx} M \propto M/\tau^2$ and $\rho^T_{yx} = R_0 \boldsymbol{B}^z_{\rm eff} \propto \tau^0$, respectively. This again ensures that ρ^T_{yx} is induced by totally different mechanism from that of the M-linear AHE, supporting our conclusion that ρ^T_{yx} originates in the effective field action due to the scalar spin chirality. The nearly T-independent behavior of ρ^T_{yx} can also be clearly discerned in the contour mapping [Fig. 3(d)]. The absolute magnitude of the observed ρ^T_{yx} ($\approx 0.16\ \mu\Omega$ cm) for MnGe is 40 times as large as that for MnSi ($\approx 0.004\ \mu\Omega$ cm [17]). This ratio appears quite reasonable; the magnetic modulation period differs in the two materials, $\lambda = 3$ nm for MnGe and $\lambda = 18$ nm for MnSi, leading the difference in the possible total spin chirality (e.g., Skyrmion density) as much as $(18/3)^2 = 36$ times.

There are supporting evidences for that a noncoplannar spin structure other than helical (conical) structure produces ρ^T_{yx} in MnGe. Shown in Fig. 4(a) is the hysteresis behavior of ρ^T_{yx} and M at 30 K. The Hall resistivity and magnetization were all measured after zero-field cooling.

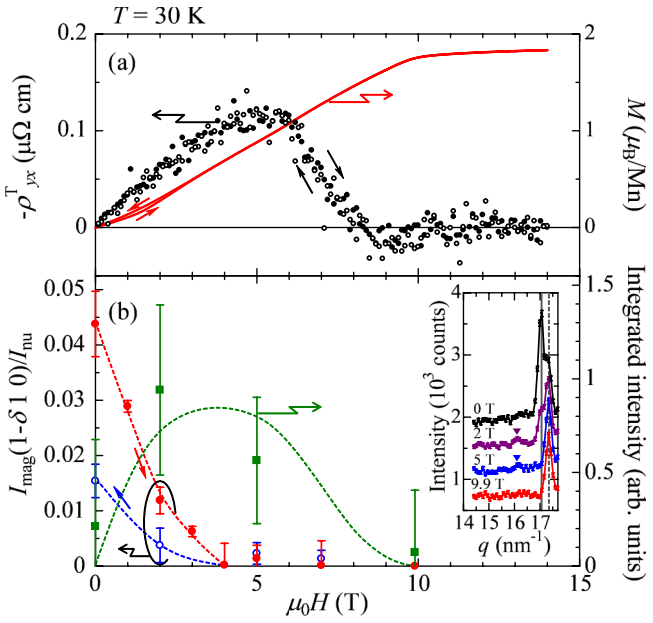

FIG. 4 (color online). Comparison between the hysteresis behavior of ρ^T_{yx}, M, and $I_{mag}(1-\delta 10)/I_{nu}$ at 30 K. $I_{mag}(1-\delta 10)$ and I_{nu} represent the neutron magnetic reflection of the screw structure and the nuclear one, respectively. Inset in panel (b) shows neutron powder diffraction patterns at 30 K at various magnetic fields. The small triangles, the solid line and the dashed line in the inset are the marks for new magnetic reflections, reflections of the helical structure, and the impurity Bragg peaks, respectively. Solid squares are the data points of the integrated intensity of the new magnetic reflection ($q = 16.1$ nm^{-1}) from the field-induced magnetic texture. Thin arrows denote directions of field scans. The dashed lines are the guide to the eyes.

Between the sequences of increasing and decreasing field, M-H curves exhibit a hysteresis. The hysteresis behavior of M in a low field region is attributable to alignment of $\boldsymbol{Q}_m$ parallel to the applied field, as generically observed for other B20-type helimagnets [26–28]: At zero-field, $\boldsymbol{Q}_m$ is pinned along ⟨111⟩ or ⟨100⟩ due to the magnetic anisotropy. With increasing field, $\boldsymbol{Q}_m$ flops along the direction of the applied field. With decreasing field after the $\boldsymbol{Q}_m$ alignment, $\boldsymbol{Q}_m$ mostly remains parallel to the field even at $H = 0$. In fact, we observed reduction of the intensity of the magnetic reflection $I_{mag}(1-\delta 10)$ after exceeding the critical field [Fig. 4(b)]. By contrast, the ρ^T_{yx}-H curves show no such field-hysteresis behavior, indicating that ρ^T_{yx} arises irrelevantly to the helical structure. In addition, as shown in Fig. 4(b), a weak, field-induced peak intensity at $q = 16.1$ nm^{-1} can be clearly observed at $\mu_0 H = 2$ T and 5 T ($< H_C$), indicating the stabilization of a new magnetic structure, e.g., Skyrmion crystal, in the magnetization process [29] as the possible origin of ρ^T_{yx}.

In conclusion, we observed the giant topological Hall effect as possibly induced by the spin chirality in the lattice-chiral magnet MnGe. The nearly temperature-independent feature of this Hall resistivity component provides a strong evidence for the spin-chirality mechanism, which may be produced via the H-induced formation of Skyrmion-like spin texture as in the other B20-type helimagnets. The large spin chirality is due to the short period (≈ 3 nm) of the magnetic structure in MnGe, which may offer further novel magnetoelectric effects.

The authors thank N. Nagaosa, J. H. Han, Y. Taguchi, S. Iguchi, S. Seki, Y. Shiomi, and T. Kurumaji for enlightening discussions. This work was partly supported by Grants-In-Aid for Scientific Research (Grant No. 22014003, 20340086, 19052004) from the MEXT of Japan, and FIRST Program by the Japan Society for the Promotion of Science (JSPS).

[1] For example, Y. Tokura and S. Seki, Adv. Mater. **22**, 1554 (2010).
[2] N. Nagaosa *et al.*, Rev. Mod. Phys. **82**, 1539 (2010).
[3] J. Ye *et al.*, Phys. Rev. Lett. **83**, 3737 (1999).
[4] M. Onoda, G. Tatara, and N. Nagaosa, J. Phys. Soc. Jpn. **73**, 2624 (2004).
[5] P. Bruno, V. K. Dugaev, and M. Taillefumier, Phys. Rev. Lett. **93**, 096806 (2004).
[6] Y. Taguchi *et al.*, Science **291**, 2573 (2001).
[7] Y. Machida *et al.*, Phys. Rev. Lett. **98**, 057203 (2007).
[8] D. Xiao, M. C. Chang, and Q. Niu, Rev. Mod. Phys. **82**, 1959 (2010).
[9] A. Bogdanov and A. Hubert, J. Magn. Magn. Mater. **138**, 255 (1994); A. Bogdanov and D. A. Yablonskii, Sov. Phys. JETP **68**, 101 (1989).
[10] U. K. Rößler, A. N. Bogdanov, and C. Pfleiderer, Nature (London) **442**, 797 (2006).
[11] B. Binz, A. Vishwanath, and V. Aji, Phys. Rev. Lett. **96**, 207202 (2006).
[12] S. Mühlbauer *et al.*, Science **323**, 915 (2009).
[13] W. Münzer *et al.*, Phys. Rev. B **81**, 041203(R) (2010).
[14] C. Pfleiderer *et al.*, J. Phys. Condens. Matter **22**, 164207 (2010).
[15] X. Z. Yu *et al.*, Nature (London) **465**, 901 (2010).
[16] X. Z. Yu *et al.*, Nature Mater. **10**, 106 (2010).
[17] A. Neubauer *et al.*, Phys. Rev. Lett. **102**, 186602 (2009).
[18] M. Lee *et al.*, Phys. Rev. Lett. **102**, 186601 (2009).
[19] Y. Ishikawa *et al.*, Solid State Commun. **19**, 525 (1976).
[20] J. Beille, J. Voiron, and M. Roth, Solid State Commun. **47**, 399 (1983).
[21] B. Lebech, J. Bernhard, and T. Freltoft, J. Phys. Condens. Matter **1**, 6105 (1989).
[22] P. Bak and M. H. Jensen, J. Phys. C **13**, L881 (1980).
[23] O. Nakanishi *et al.*, Solid State Commun. **35**, 995 (1980).
[24] H. Takizawa *et al.*, J. Solid State Chem. **73**, 40 (1988).
[25] M. Lee *et al.*, Phys. Rev. B **75**, 172403 (2007).
[26] S. V. Grigoriev *et al.*, Phys. Rev. B **73**, 224440 (2006).
[27] S. V. Grigoriev *et al.*, Phys. Rev. B **76**, 224424 (2007).
[28] M. Takeda *et al.*, J. Phys. Soc. Jpn. **78**, 093704 (2009).
[29] The observed magnetic diffractions in a magnetic field are limited in number and not enough to identify the new modulation vector.